Ranking the Importance of Nuclear Reactions for Activation and Transmutation Events

Arter, Wayne and Morgan, J. Guy and Relton,
Samuel D. and Higham, Nicholas J.

2015

MIMS EPrint: **2015.17**

ISSN 1749-9097

Ranking the Importance of Nuclear Reactions for Activation and Transmutation Events

Wayne Arter[1], J. Guy Morgan[2], Samuel D. Relton[3], and Nicholas J. Higham[4]

[1]CCFE, Culham Science Centre, Abingdon, Oxon. OX14 3DB, UK.
wayne.arter@ccfe.ac.uk
[2]Culham Electromagnetics Ltd, Culham Science Centre, Abingdon, Oxon. OX14 3DB
[3]School of Mathematics, The University of Manchester, Manchester M13 9PL
[4]School of Mathematics, The University of Manchester, Manchester M13 9PL

February 25, 2015

Abstract

Pathways-reduced analysis is one of the techniques used by the FISPACT-II nuclear activation and transmutation software to study the sensitivity of the computed inventories to uncertainties in reaction cross-sections. Although deciding which pathways are most important is very helpful in for example determining which nuclear data would benefit from further refinement, pathways-reduced analysis need not necessarily define the most critical reaction, since one reaction may contribute to several different pathways. This work examines three different techniques for ranking reactions in their order of importance in determining the final inventory, viz. a pathways based metric (PBM), the direct method and one based on the Pearson correlation coefficient. Reasons why the PBM is to be preferred are presented.

1 Introduction

FISPACT-II is a software suite for the analysis of nuclear activation and transmutation events of all kinds [1]. In ref [2] it was established that the pathways-reduced approach [3, 4] almost invariably gives very close agreement with Monte-Carlo sensitivities computed using the full or Bateman model for the evolution of the nuclear inventory of a target subject to irradiation by an imposed flux of projectile particles, always neutrons in this work. Pathways-reduced models are, following Eastwood and Morgan [3], identified by a graph-based approach which determines the key reaction pathways determining the inventory at a given time and eliminates from consideration those nuclides which do not lie on this reduced set of pathways.

The pathways-reduced metric is a sensitivity method in the respect that implicitly it selects a set of the most important nuclide reactions. A wide range of different sensitivity methods have been reviewed in the literature by nuclear industry experts Helton et al(2006) [5], see also Cacuci and Ionescu-Bujor(2004) [6, 7], and indeed general software packages are available, for example DAKOTA [8]. This work represents a comparison of three different techniques that exploit the pathways based reduction for the nuclear activation problem.

A key input to most techniques considered herein is an estimate of the uncertainty in the reaction cross-section. FISPACT-II can access uncertainty data on the vast majority or reactions in the EASY-II database [9], however no information is currently passed concerning pure decay reactions. This reflects the fact that half-lives are often very accurately known. There are other reactions in the database for which a value of zero uncertainty is found, usually indicating that no information is available. The implications for the three-way comparison exercise are discussed in Section 2.4.

To proceed further with this introduction, it is efficient to introduce the time evolution (rate or Bateman equation) for a nuclear inventory X

$$\frac{dX}{dt} = \mathsf{A}X \tag{1}$$

where X is the vector of nuclide numbers, and A is the matrix of nuclear interaction coefficients for both induced reactions and spontaneous decays. Note that one coefficient A_{ij} of A may represent several different nuclear reactions, since the equation involves an average over a spectrum of energies (of neutrons in the present work, although other elementary particles may be considered in general). Hence the term 'interaction' is used to cover all effects generating nuclide i as the child of parent j. It is worth noting that although i precedes j alphabetically, reactions throughout this work will be described by a parent-child ordering.

In general, the coefficients A_{ij} may change with time as the incident neutron flux changes. All the techniques for ranking the interactions A_{ij} are however most easily understood in the context of a single constant irradiation in the time interval $(0, t_f)$, producing an inventory $X(t_f)$. Different aspects of the inventory, such as heat production or kerma, may be studied using FISPACT-II, but for illustrative purposes it is sufficient to consider only the total activity

$$Q = \sum_k \lambda_k X_k(t_f) \tag{2}$$

where λ_k is the decay rate of the nuclide X_k; λ_k is zero for stable nuclides and $\lambda_k = \log_e 2/\tau_k$ for unstable ones, where τ_k is the half-life.

The three different ranking techniques are described in the next Section 2. There is novelty in the calculation of the direct sensitivity, in that the matrix Fréchet derivative is used in its computation, see Appendix, rather than the more usual decoupled direct method DDM of Dunker(1981) [10]. The application of the techniques to the wide range of test cases first introduced in ref [2] is illustrated in Section 3. Lastly Section 4 compares the utility of the different techniques.

2 Sensitivity Measures

2.1 Pathways Based Metric

The Pathways Based Metric (PBM) is calculated quite simply from the output of the pathways-reduced approach, which includes a listing of each pathway and its percentage contribution to the active nuclide at its termination. For a given interaction A_{ij}, all the number N_p of pathways upon which it lies are identified and the PBM calculated as

$$S^{ij}_{PBM} = \sum_{k=1}^{N_p} p_l \lambda_t X_t I_{kl} \tag{3}$$

where p_l is the fractional contribution of pathway l to the number of atoms X_t (evaluated at time t_f) in the inventory with decay rate λ_t and the indicator matrix $I_{kl} = 1$ or 0 depending whether or not a reaction contributing to the interaction lies on the pathway. This technique required special modification to Fispact-II for its implementation, which was facilitated by the object-oriented design of the Fortran-95 code. For the purposes of initial investigation, the loops which are identified by the graph-based approach used by Fispact-II are ignored.

2.2 Direct Method

The Direct Method (DM) works directly with the tensor describing the rate of variation of the nuclide X_k with respect to nuclear reaction coefficients. For initial investigative purposes it is sufficient to consider the partial derivative with respect to A_{ij}. Differentiating Eq. (1) with (i, j) regarded as fixed, gives

$$\frac{d}{dt}\left(\frac{\partial X}{\partial A_{ij}}\right) = A\frac{\partial X}{\partial A_{ij}} + \frac{\partial A}{\partial A_{ij}} X \tag{4}$$

If the sensitivity of the total activity is required, then using Eq. (2), this is

$$S^{ij}_{DM} = \sum_k \lambda_k \frac{\partial X_k(t_f)}{\partial A_{ij}} \tag{5}$$

In the decoupled direct method, Eq. (4) is solved for $\partial X_k/\partial A_{ij}$ using a method which exploits the sparseness of $\partial A/\partial A_{ij} = \delta_{ij}$ in the present context. However, it is also possible to express S_{DM} in terms of the matrix Fréchet derivative as explained in the Appendix, viz.

$$S^{ij}_{FDM}(t_f) = t_f \sum_k \lambda_k L_{\exp}(t_f \mathsf{A}, \mathsf{E}_{ij}) X(0) \tag{6}$$

where $L_{\exp}$ is the matrix Fréchet derivative as defined in the Appendix where E_{ij} is also defined. Eq. (6) defines the Fréchet direct method. Similarly to the PBM, this technique required modification of FISPACT-II to output the matrix A in a format suitable for input to MATLAB [11].

2.3 Pearson Derived Method

The Pearson technique for ranking sensitivities starts with the definition of the Pearson product-moment correlation coefficient for a set of N_s samples $\{(A_s, Q_s) : s = 1, \ldots, N_s\}$, viz.

$$r = \frac{\sum_s (Q_s - \bar{Q})(A_s - \bar{A})}{(N_s - 1)\Delta Q \Delta A} \tag{7}$$

where the suffix ij on r and A is to be understood, overbar denotes average and Δ denotes the standard deviation of the distribution so that for example

$$\bar{Q} = \frac{1}{N_s} \sum_{s=1}^{N_s} Q_s \tag{8}$$

$$\Delta Q = \sqrt{\frac{1}{(N_s - 1)} \sum_{s=1}^{N_s} [(Q_s)^2 - \bar{Q}^2]} \tag{9}$$

The coefficient r_{ij} is by definition always less than or equal to one, and a magnitude of r close to one indicates strong linear correlation.

However, it is the proportionality constant corresponding to $\partial Q / \partial A_{ij}$ that is of initial interest. Assuming

$$Q - \bar{Q} = \tilde{r}(A - \bar{A}) \tag{10}$$

and substituting in Eq. (7), it follows that

$$S_{PRD} = \tilde{r}_{ij} = r_{ij} \left(\frac{\Delta Q}{\Delta A} \right) \tag{11}$$

It follows that the output of the Monte-Carlo sensitivity calculations may be used to rank the different interactions by computing $r_{ij}/\Delta A$ (note that ΔQ is the same for all the A_{ij} variations in the standard approach described in ref [2]).

The calculation of the Pearson coefficient r is well-known to be sensitive to round-off error. To avoid modifying the software, the coefficient is computed using output values from FISPACT-II given only to 6 significant figures by default. This accuracy is the maximum that can be expected from the numerical integration of the rate equation which is is constrained to an accuracy of one part in a million. It was found that splitting the separate contributions of A_s and $\bar{A}$ to Eq. (7) led to unacceptable cancellation due to round-off effects, however if $\bar{Q}$ was not subtracted from Q_s before summation, this made negligible change in the value of r computed from Eq. (7).

2.4 Comments upon the Different Metrics

The main distinction between the PBM and the other two measures is that the pathways based method is ‘global’, capturing the whole variation of the inventory as parameters are varied, although having the disadvantage that it cannot measure sensitivity to diagonal entries of A. The other two techniques are more local, indeed the DM returns directly only a coefficient at the mean of the distribution of Q. The Pearson method is somewhere in-between, using global variations, but making a local linear assumption about the mean. This complicates the comparison in the next Section 3.

The principal comment to be made concerning the comparison is that, corresponding to the lack of sensitivity to element A_{ij} when it is zero due an absence of interaction between nuclides i and j, a large sensitivity in the local sense is inconsequential for the total activity Q. However, the two more local estimates (Eq. (5) and Eq. (11)) for $\partial Q/\partial A_{ij}$ should be directly comparable.

Main interest attaches to global measures such as S_{PBM}. The FDM approach may be used to produce an equivalent ranking by scaling by the estimated error in the coefficient, viz.

$$S^{ij}_{FDS} = S^{ij}_{FDM} \cdot \left(\frac{\epsilon_{ij}}{100}\right) \cdot \bar{A}_{ij} \tag{12}$$

where ϵ_{ij} is the percentage error in the distribution of the coefficient A_{ij}. Fispact-II returns both ϵ_{ij} and $\bar{A}_{ij}$ by combining the uncertainties in the reaction coefficients corresponding to A_{ij}.

From Eq. (11), a ranking based on the Pearson coefficient r should also be comparable to S_{PBM}, if it is scaled similarly, viz.

$$S^{ij}_{PRS} = r_{ij} \cdot \left(\frac{\epsilon_{ij}}{100}\right) \cdot \left(\frac{\bar{A}_{ij}}{\Delta A_{ij}}\right) \tag{13}$$

In practice it is found that $S^{ij}_{PRS} \approx r_{ij}$.

Note that for interactions for which no uncertainty information is available, a Pearson coefficient cannot be computed, nor is S_{FDS} useful. The coefficient S_{PBM} may be non-zero, but this relies on the interaction’s lying on a pathway important for other reasons. Interactions without accompanying uncertainty information will therefore largely be ignored in this work.

3 Sensitivity Calculations

3.1 Details of Cases

The test cases are taken from ref [2] and involve several different nuclide mixtures designed to be indicative of a wide range of activation problems, see Table 1. As indicated, all but one of the mixtures consisted of 1 kg of material subject to a neutron flux of $10^{15}\,cm^{-2}s^{-1}$, for a year, without any cooling period.

Table 1: Test cases. Each consists of numbers of atoms of the listed elements with their natural abundances of nuclides, given as percentages by mass of the whole.

Test Label	Constituents of Mixture	Sample Mass	Irradiation Period	Cooling Period	Neutron flux $cm^{-2}s^{-1}$
Alloy	Fe 40.0 : Ni 20.0 : Cr 20.0 : Mn 20.0	1 kg	1 yr	0	10^{15}
Alloy+c	Fe 40.0 : Ni 20.0 : Cr 20.0 : Mn 20.0	1 kg	1 yr	1 yr	10^{15}
Fe	Fe	1 kg	2.5 yr	0	10^{15}
LiMix	Li 40.0 : Be 30.0 : O 30.0	1 kg	1 yr	0	10^{15}
WMix	W 20.0 : Re 20.0 : Ir 20.0 : Bi 20.0 : Pb 20.0	1 kg	1 yr	0	10^{15}
Y2O3	Y 78.74 : O 21.26	1 g	300 s	0	1.116×10^{10}

Table 2: Test cases statistics. Monte-Carlo sampling by FISPACT-II has a sample size determined by the number of reactions examined.

Test Label	I, Reactions Examined	Matrix A Size	Max. N_x, Samples per Reaction	N_s, Total Sample
Alloy	84	51	640	53 760
Alloy+c	50	38	640	32 000
Fe	27	24	640	17 280
LiMix	17	21	640	10 880
WMix	71	63	640	45 440
Y2O3	13	16	2 560	33 280

The mixtures are used in six test cases, with the Alloy case extended to include a cooling phase. Each test case is run using the full TENDL 2013 data from the EASY-II database [9] with pathways analysis to identify the important reactions, the numbers of which are listed in Table 2. As in ref [2], Monte-Carlo solution of the reduced problem, investigating the distributions of the important reaction rates specified in the newer database, was then performed in the sequence of increasing sample size per reaction, $N_x = 10,\ 40,\ 160,\ \ldots$ up to the maximum value specified in the table. Indications from ref [2] and work which may be published elsewhere indicate that the pathways-reduced results agree to at least two (and often three) significant figures with those obtained by sampling the full problem, at less than a thousandth of the computational cost. As might be expected from the large maximum number of samples N_s employed, the distributions of reaction rates actually sampled usually agree in the mean to 4 significant figures with the nominal database values.

3.2 Results

This section presents results for each of the test cases in turn, in the alphabetic order specified in Table 1. For each test case there is a table of sensitivity rankings ordered by Fréchet derivative amplitude and a graph of rankings ordered by S_{PBM}. The table enables a larger range of interactions to be compared, since the graphs become hard to interpret once the number of plotted interactions exceeds about ten. Note the convention (except for the Y2O3 case) that all three methods must provide a ranking for the comparison to be plotted. So in the figures the ten highest-ranked cases plotted may actually have ranks lower than ten.

A general feature of all graphs comparing rankings by the different techniques is the symmetry about the mid-line labelled PBM. The appearance of "V" and "Λ" patterns indicates that although the more local measures may not agree with S_{PBM}, they do themselves correlate well.

For two of the test cases, Alloy+c in Section 3.2.2 and WMix in Section 3.2.5, further results of analysis are presented to help understand the effect of sampling and round-off on the calculation of S_{PRS}. In addition, a table of sensitivity rankings ordered by S_{PBM} and a graph of rankings ordered by Fréchet derivative also appear in these two sections. (This information is omitted from the other four sections Section 3.2.1, Section 3.2.3, Section 3.2.4 and Section 3.2.6 to save space.)

3.2.1 Alloy

Table 3: Alloy case. Rankings for different methods.

		Sensitivity		
Parent	Child	FDS	PBM	PRS
Fe-56	Mn-56	1	5	1
Ni-58	Ni-57	21	37	57
Mn-55	Cr-55	10	11	10
Mn-55	V-52	12	18	12
Mn-55	Mn-56	9	1	9
Cr-52	Cr-51	17	19	24
Cr-52	V-52	5	10	5
Ni-58	Co-58m	3	4	3
Mn-55	Mn-54	11	6	11
Fe-56	Fe-55	14	15	15
Ni-58	Co-57	8	9	8
Ni-60	Co-60m	4	13	4
Ni-58	Co-58	2	2	2
Ni-58	Fe-55	7	12	6
Fe-54	Cr-51	13	20	13
Cr-53	V-52	37	0	0
Cr-53	V-53	15	25	18
Fe-54	Mn-54	6	8	7
Cr-50	Cr-51	22	3	30
Fe-57	Mn-56	36	0	0
Fe-57	Mn-57	18	26	33
Ni-62	Fe-59	19	35	71
Ni-62	Co-62m	30	50	56
Ni-62	Co-61	39	79	66
Ni-62	Co-62	28	46	47
Ni-60	Co-60	16	28	14
Cr-54	Cr-55	24	22	67
Cr-54	Ti-51	27	49	26
Cr-54	V-54	25	52	50
Fe-54	Fe-55	26	14	48

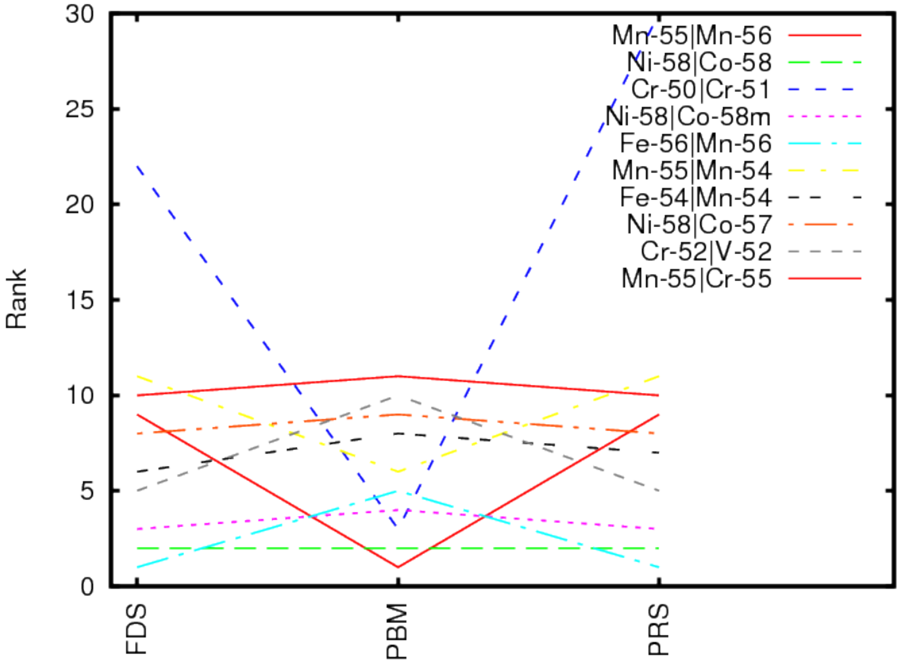

Figure 1: Comparison of the Alloy test case results, showing the first ten interactions according to the Pathways Based Metric S_{PBM}, ranked accordingly.

3.2.2 Alloy+c

Table 4 suggests that once the Pearson correlation becomes below 0.1 it becomes inaccurate. Figure 2 shows that the smaller Pearson coefficients vary erratically with sampling, from which it is inferred that round-off effects have become important.

As indicated in Table 1 this case involves both an irradiation phase and a cooling period. Care is required in comparing the FDM approach in this instance, for the method uses only the matrix for the cooling phase, whereas the other analyses are of the entire history. Although there is still reasonably good correlation between P_{FDS} and P_{PRS}, it is not as good in the other test cases.

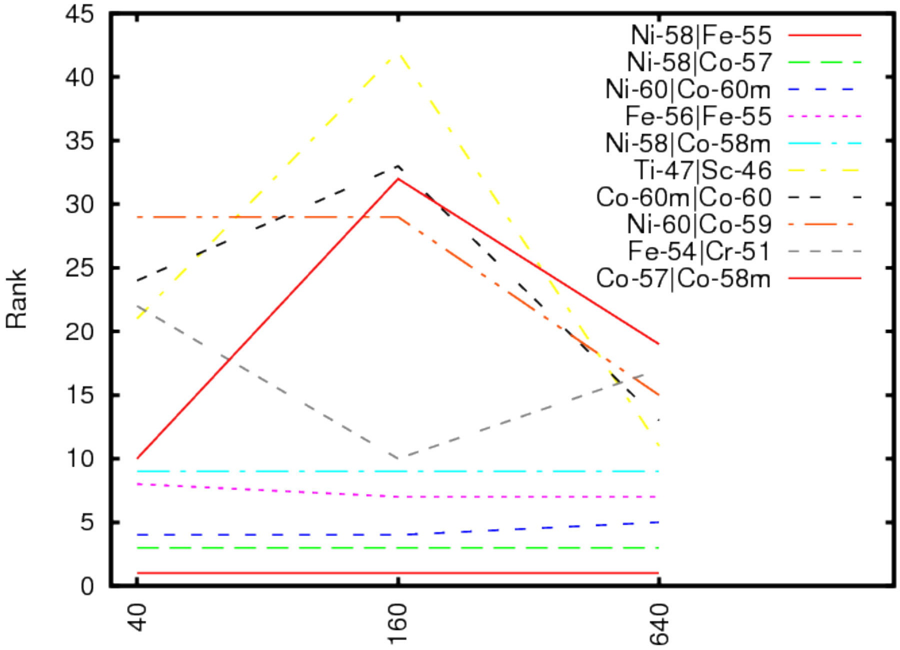

Figure 2: Comparison of the Alloy+c test case results, showing the first ten odd-numbered interactions according to the scaled Pearson technique value S_{PRS}, for a Monte-Carlo sample size of $N_x = 640$ per reaction, as N_x is increased.

Table 4: Alloy+c case. Values of absolute Pearson correlation coefficient $|r|$ as Monte Carlo sample size increases with N_x.

		Absolute Pearson		
Parent	Child	40	160	640
Ni-58	Fe-55	0.81342	0.79097	0.79709
Fe-54	Mn-54	0.48716	0.48798	0.48761
Ni-58	Co-57	0.24152	0.23469	0.23442
Mn-55	Mn-54	0.17194	0.16534	0.16563
Ni-60	Co-60m	0.16462	0.15008	0.13389
Ni-58	Co-58	0.13754	0.12544	0.11864
Fe-56	Fe-55	9.410×10^{-2}	7.202×10^{-2}	9.237×10^{-2}
Ni-60	Co-60	0.10390	6.218×10^{-2}	5.669×10^{-2}
Ni-58	Co-58m	6.996×10^{-2}	5.098×10^{-2}	4.101×10^{-2}
Ti-46	Sc-46m	3.614×10^{-2}	1.570×10^{-3}	1.575×10^{-2}
Ti-47	Sc-46	2.538×10^{-2}	2.806×10^{-3}	1.209×10^{-2}
V-49	Sc-46	4.678×10^{-3}	1.198×10^{-2}	1.144×10^{-2}
Co-60m	Co-60	1.923×10^{-2}	9.042×10^{-3}	8.303×10^{-3}
Cr-50	V-50	9.279×10^{-3}	1.598×10^{-2}	8.073×10^{-3}
Ni-60	Co-59	1.648×10^{-2}	1.167×10^{-2}	7.639×10^{-3}
Ni-57	Co-57	1.665×10^{-2}	1.499×10^{-2}	7.389×10^{-3}
Co-57	Co-58	2.483×10^{-3}	1.572×10^{-2}	6.780×10^{-3}
Fe-54	Cr-51	2.407×10^{-2}	2.252×10^{-2}	6.773×10^{-3}
Co-57	Co-58m	3.906×10^{-2}	9.176×10^{-3}	6.739×10^{-3}
Ti-47	Ti-46	2.828×10^{-2}	1.220×10^{-2}	5.516×10^{-3}
Co-59	Fe-59	8.709×10^{-3}	1.451×10^{-2}	5.499×10^{-3}
Fe-58	Fe-59	2.626×10^{-2}	1.466×10^{-2}	5.289×10^{-3}
Fe-54	Fe-55	2.698×10^{-2}	7.802×10^{-3}	5.261×10^{-3}
Co-58	Fe-58	2.502×10^{-3}	1.069×10^{-3}	5.199×10^{-3}
Ti-47	Sc-46m	4.156×10^{-3}	1.867×10^{-2}	5.039×10^{-3}
Cr-50	Cr-51	1.015×10^{-2}	2.073×10^{-3}	4.815×10^{-3}
Co-59	Co-60	1.789×10^{-2}	1.673×10^{-2}	4.743×10^{-3}
Ni-58	Ni-59	2.777×10^{-3}	1.273×10^{-2}	4.581×10^{-3}
Mn-55	Mn-56	1.473×10^{-2}	3.741×10^{-3}	4.456×10^{-3}
Co-58	Co-59	5.478×10^{-3}	6.033×10^{-4}	4.220×10^{-3}

Table 5: Alloy+c case. Rankings for different methods.

		Sensitivity		
Parent	Child	FDS	PBM	PRS
Cr-52	Cr-51	11	39	49
Mn-55	Mn-54	6	1	4
Fe-56	Fe-55	9	6	7
Ni-58	Co-57	5	3	3
Ni-58	Ni-57	16	20	42
Ni-58	Co-58	1	7	6
Ni-58	Co-58m	2	9	9
Ni-58	Fe-55	4	4	1
Fe-54	Cr-51	8	40	17
Fe-54	Mn-54	3	2	2
Cr-50	Cr-51	13	26	26
Ni-62	Fe-59	12	37	44
Ni-60	Co-60	10	14	8
Ni-60	Co-60m	7	11	5
Fe-54	Fe-55	15	5	23
Cr-50	V-49	14	16	35
Fe-58	Fe-59	18	27	22
Fe-54	Mn-53	17	18	30
Ni-60	Co-59	22	28	15
Ni-59	Co-58	21	0	0
Ni-58	Fe-54	31	0	0
Ni-59	Co-58m	23	0	0
Co-59	Fe-59	19	42	20
Co-59	Co-58	26	0	0
Fe-56	Mn-55	30	0	0
Co-59	Co-58m	25	0	0
Ni-59	Fe-55	32	0	0
Ni-62	Ni-63	27	12	33
Fe-55	Mn-54	28	0	0
Co-58	Co-57	24	30	34
Co-57	Co-56	29	44	37
Co-58	Mn-54	33	0	0
Co-58	Co-58m	20	62	0

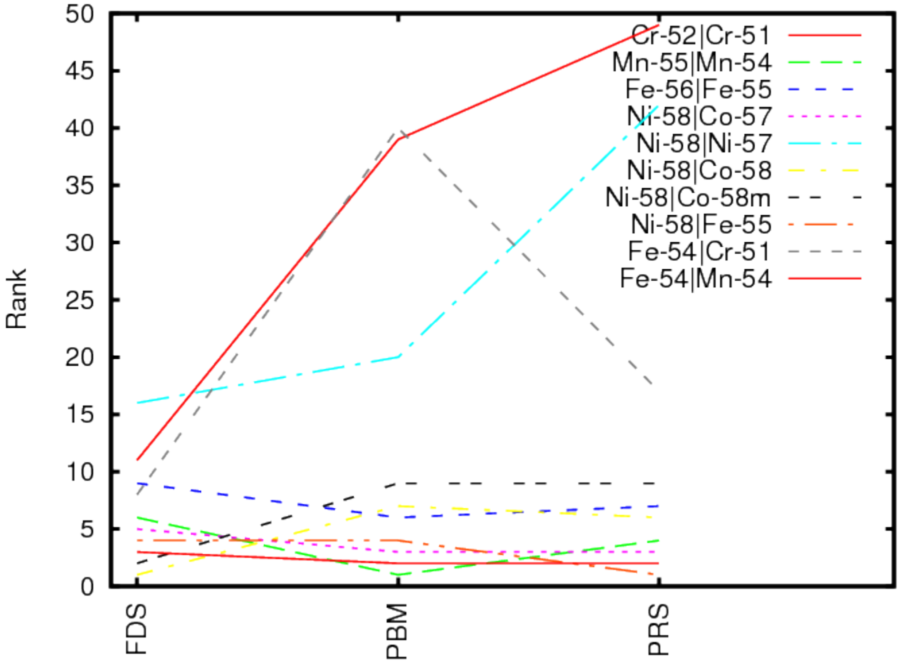

Figure 3: Comparison of the Alloy+c test case results, showing the first ten interactions by magnitude of Fréchet derivative. The labels are ordered according to Fréchet derivative size, so that the top interaction is the most sensitive.

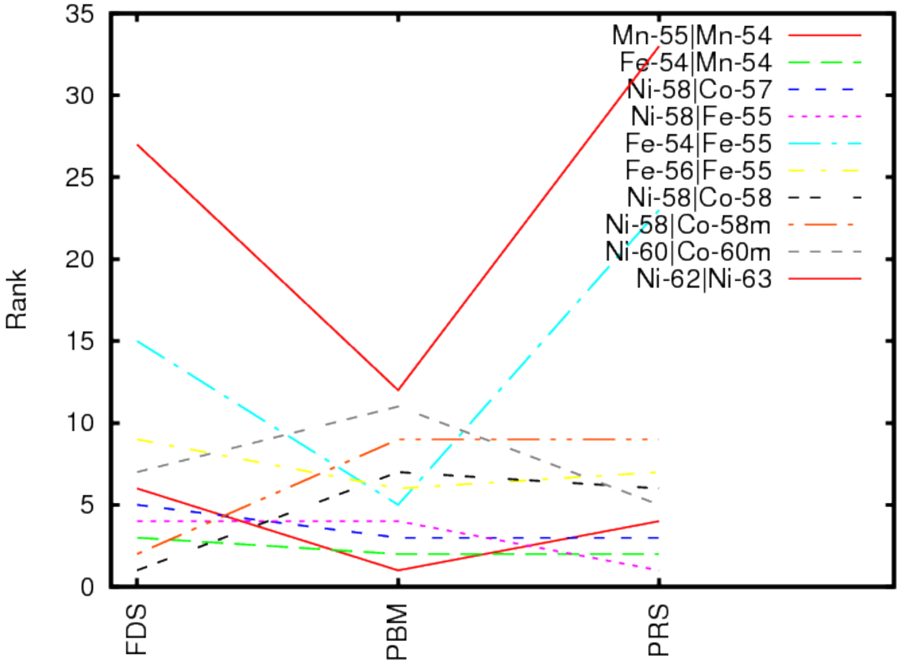

Figure 4: Comparison of the Alloy+c test case results, showing the first ten interactions according to the Pathways Based Metric S_{PBM} for which comparison is possible.

Table 6: Alloy+c case. Rankings for different methods.

		Sensitivity		
Parent	Child	FDS	PBM	PRS
Mn-55	Mn-54	6	1	4
Fe-54	Mn-54	3	2	2
Ni-58	Co-57	5	3	3
Ni-58	Fe-55	4	4	1
Fe-54	Fe-55	15	5	23
Fe-56	Fe-55	9	6	7
Ni-58	Co-58	1	7	6
Co-60m	Co-60	0	8	13
Ni-58	Co-58m	2	9	9
Co-58m	Co-58	0	10	32
Ni-60	Co-60m	7	11	5
Ni-62	Ni-63	27	12	33
Co-58	Co-59	0	13	31
Ni-60	Co-60	10	14	8
Co-59	Co-60m	0	15	43
Cr-50	V-49	14	16	35
Co-59	Co-60	0	17	27
Fe-54	Mn-53	17	18	30
Mn-53	Mn-54	0	19	46
Ni-57	Co-57	0	21	16
Ni-58	Ni-57	16	20	42
Mn-55	Mn-56	0	23	29
Mn-56	Fe-56	0	22	0
Co-58m	Co-59	0	24	36
Co-57	Co-58	0	25	18
Cr-50	Cr-51	13	26	26
Fe-58	Fe-59	18	27	22
Ni-60	Co-59	22	28	15
Ni-64	Ni-63	0	29	39
Co-58	Co-57	24	30	34

3.2.3 Fe

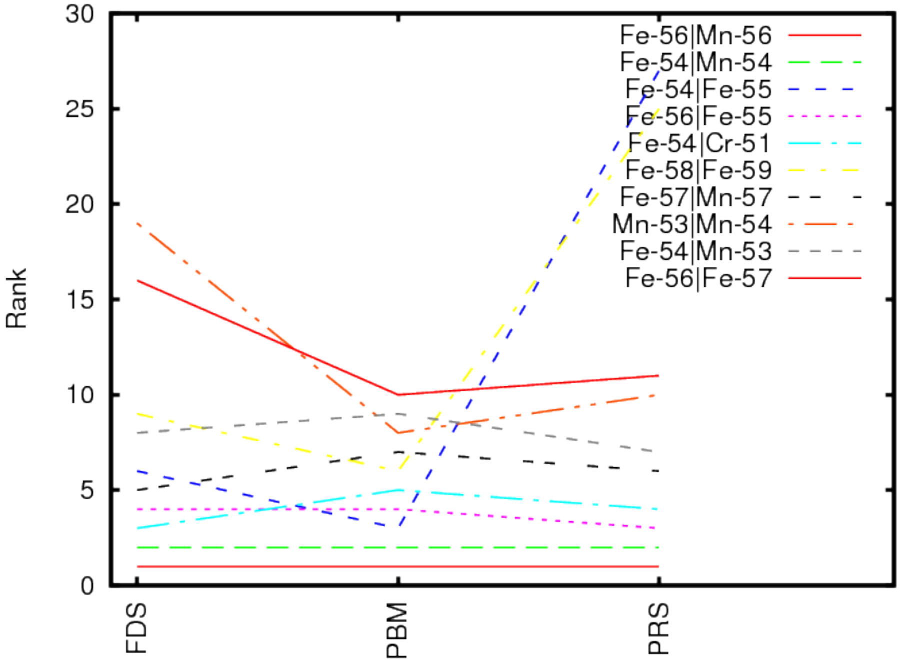

Figure 5: Comparison of the Fe test case results, showing the first ten interactions according to the Pathways Based Metric S_{PBM}, ranked accordingly.

Table 7: Fe case. Rankings for different methods.

		Sensitivity		
Parent	Child	FDS	PBM	PRS
Fe-56	Mn-56	1	1	1
Fe-56	Fe-55	4	4	3
Fe-54	Cr-51	3	5	4
Fe-54	Mn-54	2	2	2
Fe-57	Mn-56	13	0	0
Fe-57	Mn-57	5	7	6
Fe-54	Fe-55	6	3	27
Fe-56	Mn-55	7	27	18
Fe-58	Fe-59	9	6	25
Fe-58	Cr-55	10	19	8
Fe-58	Mn-58m	11	21	19
Fe-58	Mn-58	12	22	22
Fe-54	Mn-53	8	9	7
Fe-56	Fe-57	16	10	11
Fe-55	Mn-54	14	0	0
Cr-54	Cr-55	20	15	12
Cr-54	V-54	21	26	5
Mn-55	Cr-55	18	24	26
Mn-55	V-52	22	25	16
Mn-55	Mn-56	15	0	0
Fe-57	Fe-58	25	13	24
Mn-55	Mn-54	24	0	0
Fe-57	Cr-54	27	28	14
V-51	V-52	32	16	23
Mn-53	Mn-54	19	8	10
Fe-57	Fe-56	23	0	0
Co-59	Co-60m	30	12	21
Co-59	Mn-56	31	0	0
Co-59	Fe-59	28	0	0
Fe-55	Mn-55	17	23	17

3.2.4 LiMix

The comparison between the various metrics in Figure 6 does not at first appear to be as successful as in other cases. However the dominant interaction from the PBM involves tritium for which uncertainty data are not accessible in the database, hence the FDS and PRS cannot assign it a ranking and it is omitted from the plot. Moreover all FDS rankings over 21 similarly correspond to zero uncertainty and allowing for this, the comparison is as good as any reported herein.

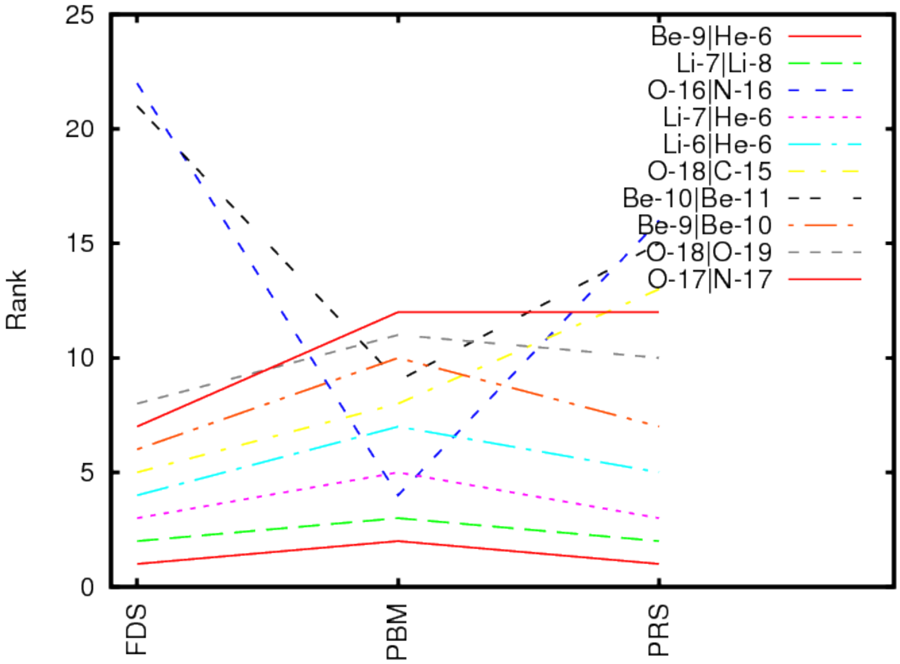

Figure 6: Comparison of the LiMix test case results, showing the first ten interactions according to the Pathways Based Metric S_{PBM} for which comparison is possible.

Table 8: LiMix case. Rankings for different methods.

		Sensitivity		
Parent	Child	FDS	PBM	PRS
Li-7	He-6	3	5	3
Li-7	Li-8	2	3	2
Be-9	He-6	1	2	1
O-16	N-16	22	4	16
Li-6	He-6	4	7	5
Li-7	Li-6	24	0	0
Be-9	Be-10	6	10	7
O-18	O-19	8	11	10
O-18	C-15	5	8	13
O-17	N-16	15	0	0
O-17	N-17	7	12	12
O-16	N-15	18	14	11
Be-9	Li-7	11	0	0
He-3	H-3	25	0	0
Be-10	He-6	27	0	0
Be-10	Be-11	21	9	15
O-16	O-17	14	18	4
Li-6	Li-7	13	0	0
N-15	N-16	19	0	0
N-15	C-15	12	0	0
N-15	B-12	9	13	6
C-13	Be-10	10	16	8
O-16	C-13	23	15	17
C-13	Be-9	26	0	0
O-17	O-18	20	0	0
O-17	N-15	17	20	9
O-17	O-16	16	0	0

3.2.5 WMix

Table 9 suggests that once the Pearson correlation becomes below 0.1 it becomes inaccurate. Figure 7 shows that the lower rankings in terms of sensitivity vary erratically with sampling for similar reasons to do with round-off effects.

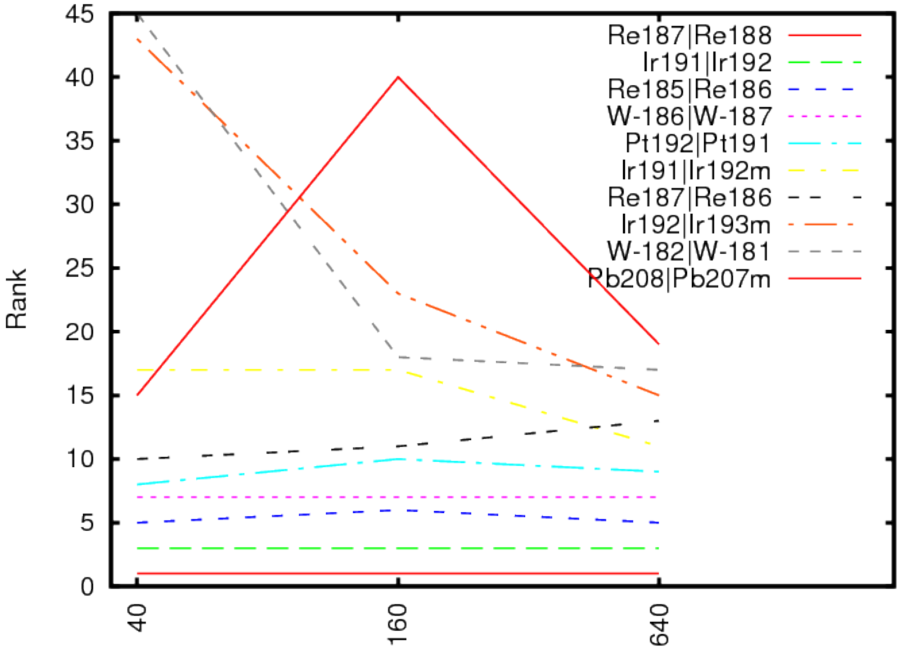

Figure 7: Comparison of the WMix test case results, showing the first ten odd-numbered interactions according to the scaled Pearson technique value S_{PRS}, for a Monte-Carlo sample size of $N_x = 640$ per reaction, as N_x is increased.

Table 9: WMix case. Values of absolute Pearson correlation coefficient $|r|$ as Monte Carlo sample size increases with N_x.

		Absolute Pearson		
Parent	Child	40	160	640
Re187	Re188	0.93702	0.94033	0.94091
Ir193	Ir194	0.24971	0.23407	0.24135
Ir191	Ir192	0.13306	0.13520	0.13542
Ir193	Ir193m	0.11155	0.11969	0.11550
Re185	Re186	0.10156	8.413×10^{-2}	7.955×10^{-2}
W-184	W-185	6.398×10^{-2}	9.215×10^{-2}	7.856×10^{-2}
W-186	W-187	5.029×10^{-2}	6.135×10^{-2}	6.423×10^{-2}
Re187	Re188m	2.181×10^{-2}	5.108×10^{-2}	5.264×10^{-2}
Pt192	Pt191	4.270×10^{-2}	4.238×10^{-2}	3.215×10^{-2}
Ir193m	Ir193	2.090×10^{-3}	9.212×10^{-3}	2.514×10^{-2}
Ir191	Ir192m	3.290×10^{-2}	1.785×10^{-2}	2.510×10^{-2}
W-186	W-185m	4.033×10^{-2}	4.676×10^{-2}	2.323×10^{-2}
Re187	Re186	3.941×10^{-2}	2.248×10^{-2}	1.720×10^{-2}
Bi209	Bi210	6.132×10^{-5}	1.141×10^{-2}	1.679×10^{-2}
Ir192	Ir193m	1.539×10^{-2}	1.425×10^{-2}	1.637×10^{-2}
Ir192	Ir193	1.845×10^{-2}	1.529×10^{-2}	1.352×10^{-2}
W-182	W-181	1.497×10^{-2}	1.685×10^{-2}	1.274×10^{-2}
Ir191	Ir190	2.775×10^{-2}	8.743×10^{-3}	1.263×10^{-2}
Pb208	Pb207m	3.345×10^{-2}	9.360×10^{-3}	1.217×10^{-2}
Ir191	Ir191m	2.715×10^{-2}	1.390×10^{-2}	1.167×10^{-2}
Pt194	Pt193m	1.482×10^{-2}	1.318×10^{-2}	1.020×10^{-2}
W-186	W-185	3.379×10^{-2}	1.427×10^{-2}	9.663×10^{-3}
W-183	W-183m	2.160×10^{-3}	1.927×10^{-2}	9.005×10^{-3}
W-183	W-184	5.385×10^{-3}	1.532×10^{-3}	8.812×10^{-3}
Ir193	Ir192	2.121×10^{-2}	8.499×10^{-3}	8.497×10^{-3}
Re185	Re184m	1.874×10^{-2}	7.629×10^{-3}	8.467×10^{-3}
Ir194	Ir195m	4.688×10^{-3}	5.884×10^{-3}	8.447×10^{-3}
Ir193	Os193	3.587×10^{-4}	2.355×10^{-3}	8.253×10^{-3}
Re188m	Re188	1.010×10^{-2}	4.477×10^{-3}	7.839×10^{-3}
Bi210m	Bi210	1.836×10^{-2}	3.068×10^{-3}	7.527×10^{-3}

Table 10: WMix case. Rankings for different methods.

		Sensitivity		
Parent	Child	FDS	PBM	PRS
Bi209	Bi210	14	38	14
Re187	W-185m	29	0	0
Re187	Re188m	6	12	8
Ir193	Os191	35	0	0
Ir193	Os191m	37	0	0
Bi209	Pb207m	28	0	0
Ir193	Ir192m	11	0	0
Re187	W-185	31	0	0
W-184	W-185m	17	50	51
Re187	W-187	19	0	0
Ir193	Ir193m	3	16	4
Re187	Ta183	32	0	0
W-186	W-185m	7	27	12
Re187	Re186	8	18	13
Re187	Re188	1	4	1
Pt194	Os191	26	0	0
Pt194	Os191m	30	0	0
Pb208	Pb207m	12	26	19
Re185	W-185m	20	0	0
Ir193	Ir192	9	20	26
W-184	W-185	4	13	6
Ir193	Ir194	2	1	2
Pt194	Ir193m	34	0	0
W-186	W-185	10	21	22
W-184	Ta183	33	0	0
W-184	Ta182m	38	0	0
W-184	Ta182	36	0	0
W-184	W-183m	15	35	55
Pt194	Ir194	24	0	0
Pt194	Pt193m	13	24	21

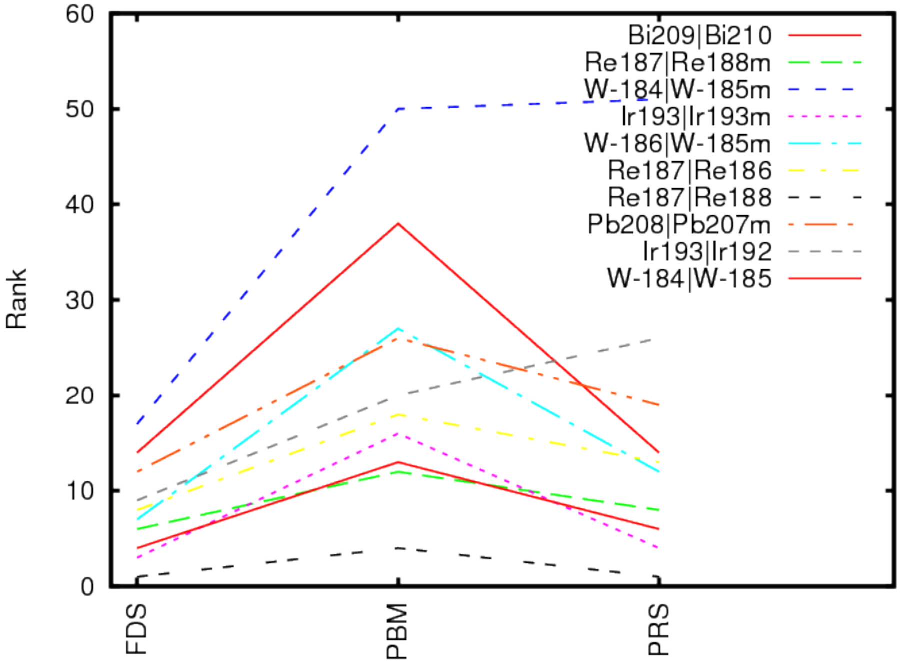

Figure 8: Comparison of the WMix test case results, showing the first ten interactions by magnitude of Fréchet derivative. The labels are ordered according to Fréchet derivative size, so that the top interaction is the most sensitive.

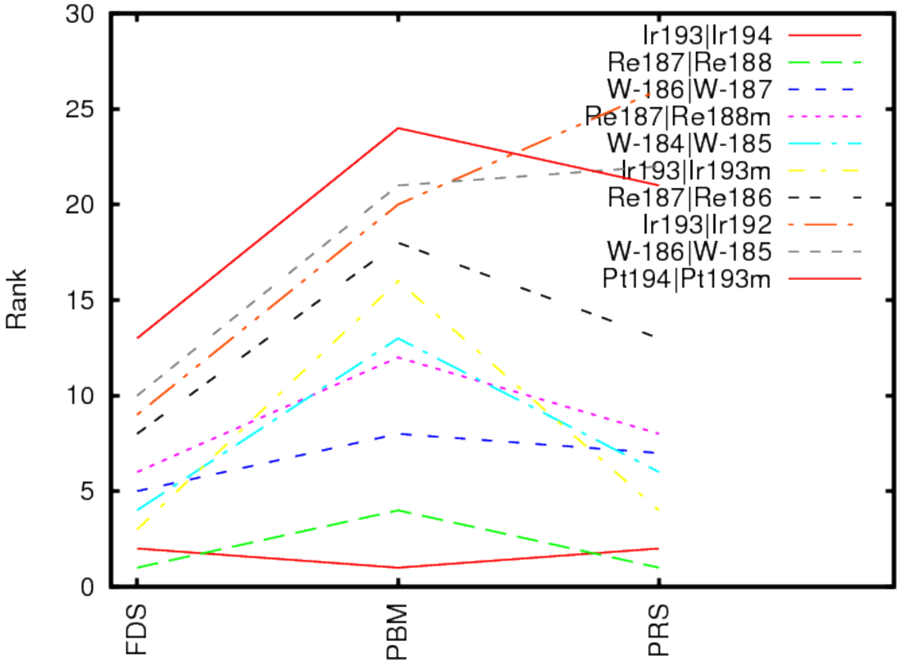

Figure 9: Comparison of the WMix test case results, showing the first ten interactions according to the Pathways Based Metric S_{PBM} for which comparison is possible.

Table 11: WMix case. Rankings for different methods.

		Sensitivity		
Parent	Child	FDS	PBM	PRS
Ir193	Ir194	2	1	2
Re185	Re186	0	2	5
Ir191	Ir192m	0	3	11
Re187	Re188	1	4	1
Ir191	Ir192	0	5	3
Ir192m	Ir192	0	6	71
Ir192	Ir193m	0	7	15
W-186	W-187	5	8	7
Ir193m	Ir193	0	9	10
Ir192	Ir193	0	10	16
W-187	Re187	0	11	0
Re187	Re188m	6	12	8
W-184	W-185	4	13	6
Re186	W-186	0	14	37
Re188m	Re188	0	15	29
Ir193	Ir193m	3	16	4
W-185	Re185	0	17	0
Re187	Re186	8	18	13
Ir194	Ir195	0	19	62
Ir193	Ir192	9	20	26
W-186	W-185	10	21	22
W-182	W-181	0	22	17
Pb207	Pb207m	0	23	54
Pt194	Pt193m	13	24	21
Ir194	Pt194	0	25	0
Pb208	Pb207m	12	26	19
W-186	W-185m	7	27	12
Ir191	Ir191m	0	28	20
Re186	Os186	0	29	0
Os186	Os185	0	30	38

3.2.6 Y2O3

The activity at the end of this test case is dominated (99.6 %) by two nuclides N-16 and Y-89m, hence all the detailed rankings by Pearson apart from the first two are suspect. It follows that although the correlation between the two methods appears poor, it is surprisingly good. The reactions O-16| N-16 and Sr-89| Y-89m have no corresponding uncertainty estimate, leading to their very high ranking values based on S_{FDS}.

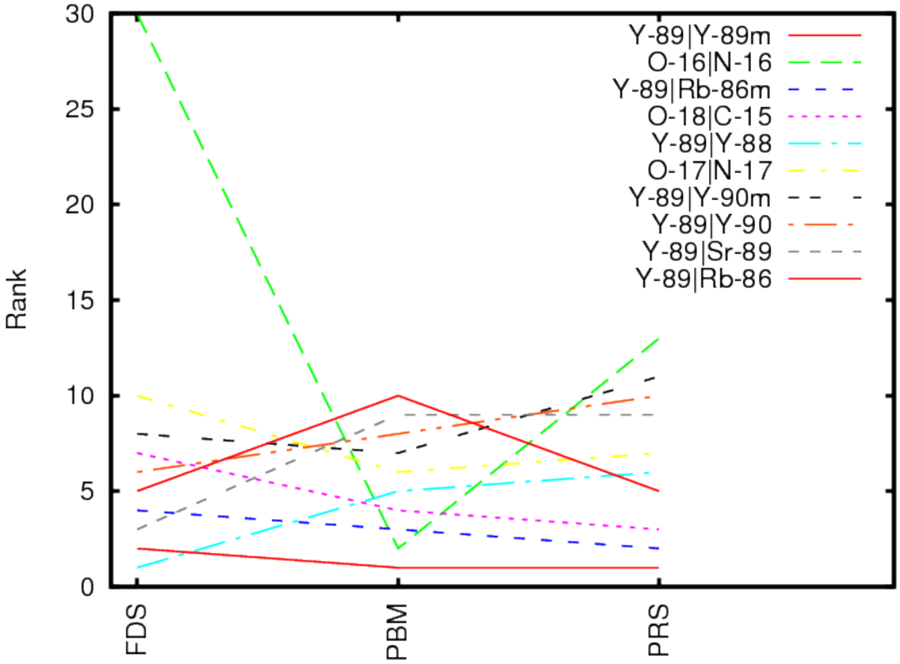

Figure 10: Comparison of the Y2O3 test case results, showing the first ten interactions according to the Pathways Based Metric S_{PBM}, for which comparison is possible.

Table 12: Y2O3 case. Rankings for different methods.

		Sensitivity		
Parent	Child	FDS	PBM	PRS
Y-89	Y-90m	8	7	11
Y-89	Rb-86m	4	3	2
O-16	N-16	30	2	13
Y-89	Rb-86	5	10	5
Y-89	Y-89m	2	1	1
Y-89	Y-90	6	8	10
Y-89	Sr-89	3	9	9
Y-89	Y-88	1	5	6
O-18	N-16	11	0	0
O-18	C-15	7	4	3
O-18	N-17	12	11	12
O-17	N-16	9	0	0
O-17	N-17	10	6	7
Y-88	Y-89m	13	0	0
O-16	O-17	15	0	0
Sr-89	Y-89m	31	0	0
Rb-86	Rb-86m	14	0	0
O-18	O-16	21	0	0
Y-90	Y-90m	18	0	0
Y-90	Rb-86m	23	0	0
O-18	O-17	16	0	0
O-17	O-18	24	0	0
Y-90	Rb-86	22	0	0
Y-90	Y-89m	19	0	0
Y-90	Sr-89	20	0	0
O-17	O-16	17	0	0
Y-89m	Y-90m	28	0	0
Y-89m	Rb-86m	26	0	0
Y-89m	Rb-86	27	0	0
Y-89m	Y-90	29	0	0
Y-89m	Sr-89	25	0	0

4 Conclusions

The sensitivity of the total activity of an inventory to uncertainties in the nuclear data for neutron-induced reactions has been studied. Six different test cases covering nearly the whole range of atomic masses were considered using three different ranking techniques. It is expected that similar results would be obtained for other inventory properties and other particle species.

The principal result is that a simple pathways based metric (PBM) gives a sensitivity ranking of interactions which is comparable to ranking based on more conventional measures obtained either by the direct method or in terms of Pearson correlation coefficients. Moreover, the PBM is superior in that it

1. is quick to calculate once the principal pathways have been identified
2. does not suffer from numerical difficulties such as underflow (Fréchet direct) or round-off (Pearson) in its evaluation
3. may be generalised to the case of multiple irradiation periods just like the pathways-reduced approach itself, whereas the other two techniques require further investigation.
4. does not require error estimates for every interaction coefficient like Pearson.

An additional noteworthy feature is that the PBM, which is a global measure of uncertainty, is *comparable* with more local measures, provided these others are scaled by the uncertainty in the reaction cross-section. This scaling is to be expected since the uncertainty estimates computed by FISPACT-II [1, § A.13] involve a multiplication by a measure of cross-section uncertainty (r.m.s. is used to combine reaction coefficients rather than the simple percentages). However, the product also involves the number of child nuclides in the inventory which is a significantly different measure from the point sensitivity measures.

The value of studying a wide range of test cases is that it demonstrates the general applicability of the above conclusions. In conjunction with modifications to FISPACT-II for more efficient pathways-based analysis in the presence of multiple irradiations, the PBM should be extended to account for loops in the pathways and ultimately integrated into a production version of the FISPACT-II package.

Acknowledgement

We are grateful to our colleagues J.-C.Sublet and J.W.Eastwood for much advice and assistance. This work has been funded by the RCUK Energy Programme under grant number EP/I501045. To obtain further information on the data and models underlying this paper please contact PublicationsManager@ccfe.ac.uk. The work of Relton and Higham was supported by European Research Council Advanced Grant MATFUN (267526) and Engineering and Physical Sciences Research Council grant EP/I03112X/1.

Appendix: Fréchet Derivatives

As explained in Section 1, the Bateman equation Eq. (1)

$$\frac{dX}{dt} = \mathsf{A}X, \quad X(0) = X_0, \quad t \in [0, t_f]\,,$$

where $X \in \mathbb{R}^n$ is a vector of nuclide numbers and $\mathsf{A} \in \mathbb{R}^{n\times n}$ is a matrix of nuclear interaction coefficients, controls the evolution of the nuclear activation over time. In this appendix, we focus on the case where A is constant in time.

We are interested in the sensitivity of the total activity Eq. (2)

$$Q = \sum_{k=1}^{n} \lambda_k X_k(t_f)$$

to the elements in A, which is determined by the n^2 numbers $\partial Q/\partial A_{ij}$. To determine these quantities we use the matrix exponential and its Fréchet derivative. The matrix exponential of $\mathsf{A} \in \mathbb{R}^{n\times n}$ is defined by

$$e^{\mathsf{A}} = \sum_{k=1}^{\infty} \frac{\mathsf{A}^k}{k!}.$$

The Fréchet derivative of the exponential at A in the direction $\mathsf{E} \in \mathbb{R}^{n\times n}$ is denoted by $L_{\exp}(\mathsf{A}, \mathsf{E}) \in \mathbb{R}^{n\times n}$ and satisfies

$$e^{\mathsf{A}+\mathsf{E}} = e^{\mathsf{A}} + L_{\exp}(\mathsf{A}, \mathsf{E}) + o(\|\mathsf{E}\|)\,.$$

For further details of Fréchet derivatives see [12, Chap. 3].

The solution to the Bateman equation is given by

$$X(t) = e^{\mathsf{A}t} X_0$$

and so

$$Q = f^T X(t_f) = f^T e^{\mathsf{A}t_f} X_0, \qquad f = [\lambda_1 \ldots \ \lambda_n]^T\,.$$

Let E_{ij} be the $n \times n$ matrix with a 1 in the (i, j) entry and zeros elsewhere. Now,

$$\begin{aligned}
\frac{\partial Q}{\partial A_{ij}} &= \lim_{\delta\to 0} \frac{Q(A_{ij} + \delta) - Q(A_{ij})}{\delta} \\
&= \lim_{\delta\to 0} \frac{f^T \left(e^{(\mathsf{A}+\mathsf{E}_{ij}\delta)t_f} - e^{\mathsf{A}t_f}\right) X_0}{\delta} \\
&= \lim_{\delta\to 0} \frac{f^T \left(L_{\exp}(\mathsf{A}t_f, \mathsf{E}_{ij}t_f\delta) + o(\delta)\right) X_0}{\delta} \\
&= t_f f^T L_{\exp}(\mathsf{A}t_f, \mathsf{E}_{ij}) X_0,
\end{aligned}$$

where we have used the fact that $L_{\exp}$ is linear in its second argument.

To determine the k largest of these derivatives we can simply compute them all and sort them. For this we can use the relationship [12, eq. (3.16)]

$$\exp\left(\begin{bmatrix} t\mathsf{A} & \mathsf{E}_{ij} \\ 0 & t\mathsf{A} \end{bmatrix}\right) = \begin{bmatrix} e^{t\mathsf{A}} & L_{\exp}(t\mathsf{A}, \mathsf{E}_{ij}) \\ 0 & e^{t\mathsf{A}} \end{bmatrix}, \tag{14}$$

which yields the formula

$$\exp\left(\begin{bmatrix} t\mathsf{A} & \mathsf{E}_{ij} \\ 0 & t\mathsf{A} \end{bmatrix}\right) \begin{bmatrix} 0 \\ X_0 \end{bmatrix} = \begin{bmatrix} L_{\exp}(t\mathsf{A}, \mathsf{E}_{ij})X_0 \\ e^{t\mathsf{A}}X_0 \end{bmatrix}. \tag{15}$$

Hence one method to compute $L_{\exp}(\mathsf{A}t_f, \mathsf{E}_{ij})X_0$ is to apply the method from [13] to compute the product on the left-hand side and then read off the first n components.

However, it is not necessary to carry out n^2 Fréchet derivative evaluations. One suffices, as we now explain. We need some notation. The Kronecker product of two matrices B and C (of any dimension) is the block matrix $\mathsf{B} \otimes \mathsf{C} = (b_{ij}\mathsf{C})$. The vec operator stacks the columns of a matrix one of top of each other from first to last, producing a long vector. We need the property that $\mathrm{vec}(L_{\exp}(\mathsf{A}, \mathsf{E})) = \mathsf{K}(\mathsf{A})\,\mathrm{vec}(\mathsf{E})$, for some $n^2 \times n^2$ matrix $\mathsf{K}(\mathsf{A})$ that satisfies $\mathsf{K}(\mathsf{A})^T = \mathsf{K}(\mathsf{A}^T)$. Using the fact that the vec of a scalar is itself and the formula

$$\mathrm{vec}(\mathsf{AXB}) = (\mathsf{B}^T \otimes \mathsf{A})\,\mathrm{vec}(\mathsf{X}),$$

we have

$$\begin{aligned} \frac{\partial Q}{\partial A_{ij}} &= t_f f^T L_{\exp}(\mathsf{A}t_f, \mathsf{E}_{ij})X_0 \\ &= \mathrm{vec}\left(t_f f^T L_{\exp}(\mathsf{A}t_f, \mathsf{E}_{ij})X_0\right) \\ &= t_f (X_0 \otimes f)^T \,\mathrm{vec}\left(L_{\exp}(\mathsf{A}t_f, \mathsf{E}_{ij})\right) \\ &\equiv t_f g^T \mathsf{K}(\mathsf{A}t_f)\,\mathrm{vec}(\mathsf{E}_{ij}), \end{aligned}$$

where $g = X_0 \otimes f$. Now, since $\mathrm{vec}(\mathsf{E}_{ij})$ is a unit vector, we simply require the k largest elements in modulus of $g^T\mathsf{K}(\mathsf{A}t_f)$, which are the largest k elements in magnitude of $\mathsf{K}(\mathsf{A}t_f)^T g$. We have $\mathsf{K}(\mathsf{A}^T t_f)g = \mathrm{vec}(L_{\exp}(\mathsf{A}^T t_f, \mathsf{E}))$, where $\mathrm{vec}(\mathsf{E}) = g = X_0 \otimes f$ and hence $\mathsf{E} = f x_0^T$. This means that a single Fréchet derivative evaluation is sufficient, and it can be done using the relationship (14) above with an algorithm to compute the matrix exponential such as that in [14].

Some of the matrices arising from nuclear activation problems can be susceptible to underflow and overflow, due to the large range of magnitudes in the coefficients. This may necessitate the use of quadruple precision arithmetic on certain problems. Quadruple precision was used to check the accuracy of all the Fréchet derivatives calculated in the course of the current work.

References

[1] Sublet, J.-C. and Eastwood, J.W. and Morgan, J.G. The FISPACT-II User Manual. Issue 6. Technical Report CCFE-R(11)11, CCFE, June 2014.

[2] Arter, W. and Morgan, J.G. Sensitivity analysis for activation problems. In *Joint International Conference on Supercomputing in Nuclear Applications and Monte Carlo 2013*, page 02404, 2014. http://dx.doi.org/10.1051/snamc/201402403.

[3] Eastwood, J.W. and Morgan, J.G. Pathways and uncertainty prediction in FISPACT-II. In *Joint International Conference on Supercomputing in Nuclear Applications and Monte Carlo 2013*, 2013. http://dx.doi.org/10.1051/snamc/201402404.

[4] J.W. Eastwood, J.G. Morgan, and J.-C. Sublet. Inventory uncertainty quantification using TENDL covariance data in Fispact-II. *Nuclear Data Sheets*, 123:84–91, 2015.

[5] J.C. Helton, J.D. Johnson, C.J. Sallaberry, and C.B. Storlie. Survey of sampling-based methods for uncertainty and sensitivity analysis. *Reliability Engineering & System Safety*, 91(10–11):1175–1209, 2006.

[6] M. Ionescu-Bujor and D.G. Cacuci. A comparative review of sensitivity and uncertainty analysis of large-scale systems. I: Deterministic methods. *Nuclear Science and Engineering*, 147(3):189–203, 2004.

[7] D.G. Cacuci and M. Ionescu-Bujor. A comparative review of sensitivity and uncertainty analysis of large-scale systems. II: Statistical methods. *Nuclear Science and Engineering*, 147(3):204–217, 2004.

[8] B.M. Adams, M.S. Ebeida, M.S. Eldred, J.D. Jakeman, L.P. Swiler, J.A. Stephens, D.M. Vigil, T.M. Wildey, W.J. Bohnhoff, K.R. Dalbey, J.P. Eddy, , K.T. Hu, L.E. Bauman, and P.D. Hough. DAKOTA, A Multilevel Parallel Object-Oriented Framework for Design Optimization, Parameter Estimation, Uncertainty Quantification, and Sensitivity Analysis: Version 6.0 User's Manual. Technical report, Sandia Technical Report SAND2014-4633, Sandia National Laboratories, Albuquerque, NM, 2014.

[9] EASY-II European Activation System. http://www.ccfe.ac.uk/EASY.aspx.

[10] A.M. Dunker. Efficient calculation of sensitivity coefficients for complex atmospheric models. *Atmospheric Environment*, 15(7):1155–1161, 1981.

[11] The MathWorks. *MATLAB*. The MathWorks, Inc., Natick, Massachusetts, United States, Release 2012a.

[12] Nicholas J. Higham. *Functions of Matrices: Theory and Computation*. Society for Industrial and Applied Mathematics, Philadelphia, PA, USA, 2008.

[13] Awad H. Al-Mohy and Nicholas J. Higham. Computing the action of the matrix exponential, with an application to exponential integrators. *SIAM J. Sci. Comput.*, 33(2):488–511, 2011.

[14] Awad H. Al-Mohy and Nicholas J. Higham. A new scaling and squaring algorithm for the matrix exponential. *SIAM J. Matrix Anal. Appl.*, 31(3):970–989, August 2009.